ChemPubSoc Europe

DOI: 10.1002/ejic.201600510

EurJIC European Journal of Inorganic Chemistry

Full Paper

Water Oxidation Catalysts

Multifaceted Bicubane Co_4 Clusters: Magnetism, Photocatalytic Oxygen Evolution, and Electrical Conductivity

Wan-Feng Xie,[a,b][‡] Ling-Yu Guo,[a][‡] Jia-Heng Xu,[a][‡] Marko Jagodič,[c] Zvonko Jagličić,[c] Wen-Guang Wang,[a] Gui-Lin Zhuang,[d] Zhi Wang,[a] Chen-Ho Tung,[a] and Di Sun*[a]

Abstract: The use of 1-(hydroxymethyl)-3,5-dimethylpyrazole (HL), a functionalized pyrazole ligand, to assemble with CoX_2 (X = Cl or Br) in the presence of triethylamine under low-temperature solvothermal conditions gave rise to two tetranuclear cobalt(II) clusters, $[Co_4L_6X_2]$ [X = Cl (**1**), Br (**2**)]. Both Co^{II}_4 clusters are isostructural and protected by four μ_2-N^1:O^2 and two μ_3-N^1:O^3L^- as well as terminal X anions to form a face-shared open bicubane structural motif. Magnetic susceptibility measurements indicated that there is an intramolecular antiferromagnetic interaction between four Co^{II} atoms in **1** and **2**. Although the core motif of **1** and **2** is not classic Co_4O_4 monocubane, both are active catalysts for water oxidation, and their relative O_2-evolution rates are dependent on the halogen terminal ligands, which is also supported by spin-polarized density functional theory (DFT) calculations. Both clusters exhibit semiconductor behavior with σ values on the 10^{-9} S cm^{-1} scale at room temperature; however, mechanical iodine doping results in up to an astonishing 10^5-fold maximum enhancement of solid-state conductivity relative to the undoped samples. This work therefore presents a new core type of cobalt cluster that possesses photocatalytic oxygen-evolution capabilities, provides new insight into the catalysis-related mechanism based on the relative oxygen-evolution efficiency, and applies the iodine-doping strategy to boost the conductivity of cluster compounds.

Introduction

Molecular clusters with multiple-spin metal centers have received considerable attention because of their molecular aesthetics as well as some promising applications in quantum computation,[1] molecular spintronics,[2] magnetic cooling,[3] and nanoscale magnets.[4] Undoubtedly, this field is witnessing its greatest period of success along with some record-breaking nuclearity of transition-metal clusters such as Mn_{84}, Fe_{168}, Co_{36}, Ni_{34}, Cu_{44}, Er_{60}, $La_{76}Ni_{60}$, $Cu_{17}Mn_{28}$, and $Fe_{16}Ln_4$.[5] In the face of such rich achievements, the direction in which transition-metal clusters should go to retain their vitality is a huge challenge.

Thanks to recent research on mimics of photosynthetic systems, polynuclear transition-metal clusters have restored confidence in functional materials as solar water-splitting catalysts.[6] Several X-ray structural studies[7] confirmed that an Mn_4CaO_5 cluster is the key site for the natural photosystem II (PSII) responsible for biocatalytic water oxidation. Thus, the mimics of this structural motif – that is, twisted cubane with three Mn atoms and one Ca atom occupying four corners, and a fourth Mn atom outside the cubane bridged by two oxo bridges – is an ideal pursued by synthetic chemists.[8] The most important breakthrough has been the successful synthesis of $[Mn_4CaO_4(t\mathrm{BuCO_2})_8(t\mathrm{BuCO_2H})_2(py)]$ (py = pyridine),[9] which has thus far found its best structural match in the full site of the Mn_4CaO_5 cluster in PSII. Although structural mimics of oxygen-evolving complexes (OECs) have undergone huge advances, the exploration of efficient and well-defined molecular catalysts for water oxidation is still appealing. Recently cobalt-based molecular catalysts, a strong competitive alternative to noble-metal-based catalysts,[10] have proven to be promising catalysts for water oxidation.[11] Among these molecular materials, the characteristic Co_4O_4 cubane core was considered to be the crucial active center for efficient catalysis of water oxidation[12] as seen in inorganic polyoxometalate (POM) cobalt complexes. Recently, Dismuke's group also compared the rates of water oxidation by six cobalt clusters with four different Co_xO_y cores and claimed that Co_4O_4 was the best.[13] But is the Co_4O_4 motif really the sole criterion for assessing catalytic activity toward water oxidation for the cobalt cluster family? To determine the answer, it is worth exploring new cobalt clusters with different Co_xO_y cores, then comparing their catalytic performance in water oxidation, which would not only highlight the water oxidation

[a] *Key Lab for Colloid and Interface Chemistry of Education Ministry, School of Chemistry and Chemical Engineering, Shandong University, Jinan 250100, People's Republic of China*
E-mail: dsun@sdu.edu.cn
http://www.researcherid.com/rid/G-3352-2010
[b] *School of Physics, Shandong University, Jinan 250100, People's Republic of China*
[c] *Faculty of Civil and Geodetic Engineering & Institute of Mathematics, Physics and Mechanics, University of Ljubljana, Jamova 2, 1000 Ljubljana, Slovenia*
[d] *College of Chemical Engineering and Materials Science, Zhejiang University of Technology, Hangzhou 310032, People's Republic of China*
[‡] These authors contributed equally to this work.
Supporting information and ORCID(s) from the author(s) for this article are available on the WWW under http://dx.doi.org/10.1002/ejic.201600510.

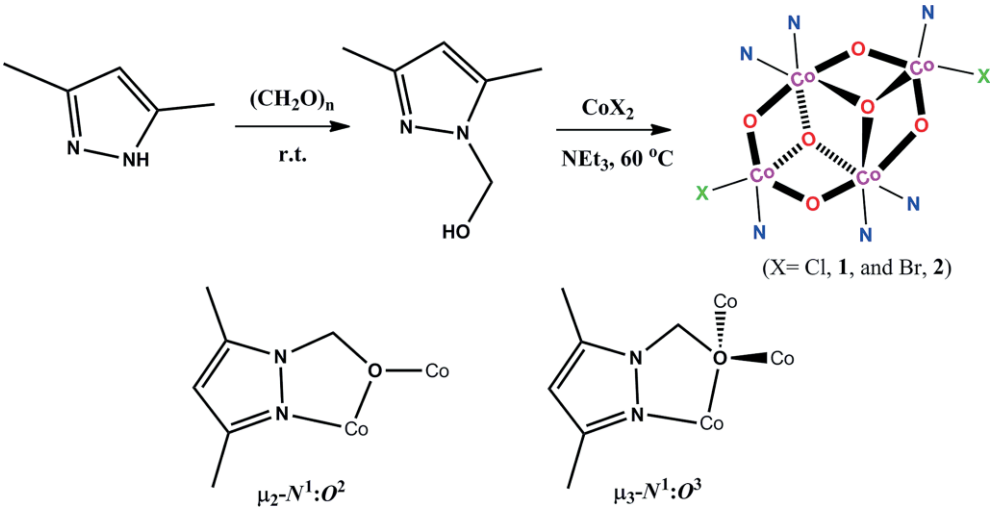

Scheme 1. Schematic representation of ligand synthesis, assembly of $[Co_4L_6X_2]$ [X = Cl (**1**), Br (**2**)] and ligand bonding mode.

chemistry of Co-OECs but might also be helpful in providing insight into the mechanism of OECs in PSII.

The hydroxymethyl-pyrazole ligand contains both pyrazole N and methoxy O coordination atoms. For this reason, it should possess excellent potential as a bridging ligand in the construction of polynuclear metal clusters. However, its usage in polynuclear metal clusters has been rare (e.g., Co^{II}, Ni^{II}, Cu^{II} clusters[14]), which might be due to the instability that is related to the decomposition reverse reaction, especially in the presence of a Cu^{II} atom.[15] For this purpose, we used 1-(hydroxymethyl)-3,5-dimethylpyrazole (HL) to construct two isostructural tetranuclear cobalt(II) clusters, $[Co_4L_6X_2]$ [X = Cl (**1**), Br (**2**)], which have the face-shared open bicubane Co_4O_6 structural motif but with different halogen anion ligands (Scheme 1). Magnetic susceptibility measurements indicated an intramolecular antiferromagnetic interaction between four Co^{II} atoms in **1** and **2**. Although the core motif of **1** and **2** is not classic Co_4O_4 monocubane, both of them are intrinsically active catalysts for water oxidation, and their relative O_2-evolution rates are dependent on the terminal halogen ligands. Interestingly, the iodine-doping strategy effectively enhanced the electrical conductivity of these tetranuclear Co clusters.

Results and Discussion

Synthetic Aspects and General Characterization

As we know, most cobalt clusters are synthesized by means of room-temperature solution reactions[16] or high-temperature solvothermal reactions (>100 °C)[17] between Co^{II} salts and ligands. However, these two cobalt clusters were synthesized by means of low-temperature solvothermal reactions, which is uncommon in the synthesis of discrete molecular clusters. We adopted this eclectic tactic mainly to avoid decomposition of the HL ligand at high temperature and to facilitate its crystallization at the same time. Comparative PXRD patterns (Figure S1 in the Supporting Information) indicated that both compound **1** and **2** were pure phases for the subsequent characterizations. Their TGA curves (Figure S2 in the Supporting Information) show three similar weight-loss steps; the first weight loss for **1** and **2** occurs at 169 and 198 °C, respectively, which indicates that complex **2** has higher thermal stability than **1**.

Cluster Structures of $[Co_4L_6X_2]$ [X = Cl (1), Br (2)]

As indicated by X-ray single-crystal diffractions, clusters **1** and **2** both crystallize in the monoclinic $P2_1/n$ space group; each asymmetric unit contains half of a complete molecule that sits on the crystallographic inversion center (Figure 1). They have very similar defect double-cubane structures. Two Co^{II} atoms (Co1 and Co1^{i}) adopt an octahedral coordination environment completed by two pyrazolyl N atoms from two L^- and four methoxy O atoms from four L^-, whereas the remaining two Co^{II} atoms (Co2 and Co2^{i}) are coordinated by three methoxy O atoms from three L^-, one pyrazolyl N atom, and one Cl or Br anion to give Co2 a trigonal-bipyramidal geometry (τ_5 = 0.95 for **1** and 0.94 for **2**).[18] The Co–O and Co–N bond lengths are 1.9631(19)–2.2918(17) and 2.052(2)–2.164(2) Å in **1** and 1.954(3)–2.266(3) and 2.052(4)–2.164(4) Å in **2**. The larger radius of Br^- with respect to that of Cl^- results in longer Co–Br bonds [2.4750(9) Å] with respect to the Co–Cl in **1** [2.3198(9) Å]. Both Co^{II}_4 clusters are protected by four μ_2-N^1:O^2 and two μ_3-N^1:O^3 L^- as well as terminal X anions to form a Co_4O_4 core, which could be described as two defect Co_3O_4 cubane subunits fused together by sharing a Co_2O_2 face. The Co···Co separations between neighboring atoms are in the ranges of 3.2069(5)–3.3144(8) Å and 3.1911(10)–3.3200(15) Å for **1** and **2**, respectively. The structures of **1** and **2** are not common in the Co cluster family and share similarities with only three complexes,

$[Co_4(OC_2H_4OEt)_6Cl_2]$ (HOC_2H_4OEt = 2-ethoxyethanol),[19] $[Co_4(hqdH)_6Cl_2]$ (hqd = 8-hydroxyquinaldine),[20] and $[Co_4(L_1)_6Cl_2]$ (HL_1 = pyridine-2-ylmethanol).[21]

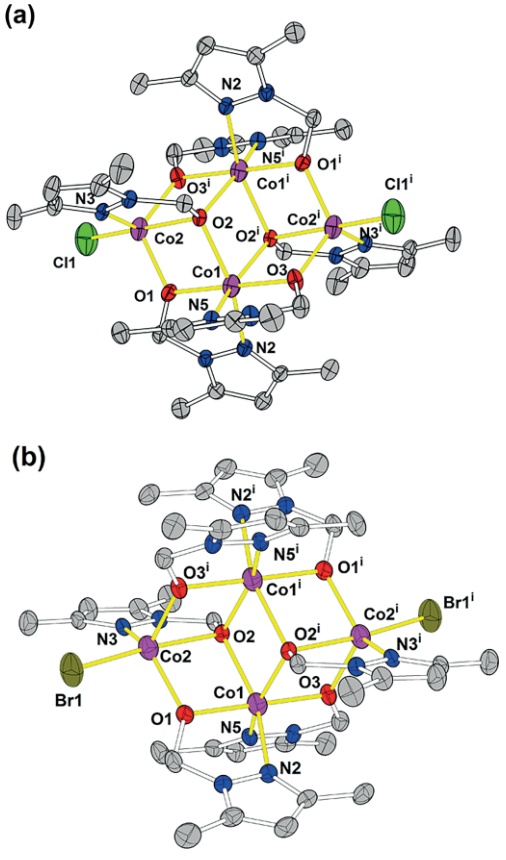

Figure 1. Labeled ORTEP (50 % probability) representation of clusters (a) **1** and (b) **2**. Hydrogen atoms are omitted for clarity. Symmetry code i: (i) –*x*, –*y* + 1, –*z*.

Magnetic Properties

Magnetic susceptibility $\chi = M/H$ was investigated between 1.8 and 300 K under a constant magnetic field H = 1000 Oe; isothermal magnetization M was measured up to 70 kOe at several temperatures below 8 K by using a Quantum Design MPMS-XL-7 SQUID magnetometer. The data were corrected for sample holder contribution and a temperature-independent magnetic susceptibility of inner-shell electrons (Larmor diamagnetism) as obtained from Pascal's tables.[22]

The product of χT (Figure 2, a) is almost the same for both **1** and **2** and practically constant between 300 and 100 K. Its value at room temperature is 2.72 emu K mol^{-1} Co, and its effective magnetic moment per Co atom is $\mu_{eff} = \sqrt{8\chi T} = 4.7\ \mu_B$. This value is larger than the high-spin-only S = 3/2 system value (3.9 μ_B) but is almost equal to 4.8 μ_B, which is the value that is typically measured for a S = 3/2 Co^{II} ion in the $3d^7$ electron configuration with non-zero orbital contribution to the magnetic moment.[23]

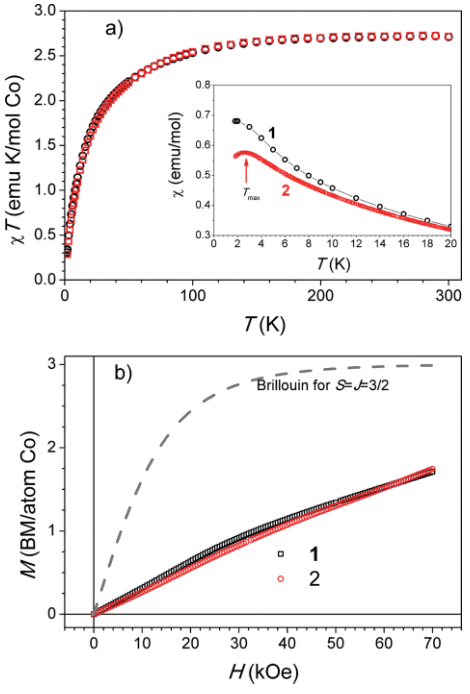

Figure 2. (a) Susceptibility (inset) and product χ·T as a function of temperature in H = 1000 Oe. (b) Magnetization curves at 1.8 K.

Below 100 K the product χT gradually decreases and finally reaches a value of 0.31 emu K mol^{-1} at 1.8 K for both **1** and **2**, which indicates an antiferromagnetic interaction between the Co^{II} ions. The existence of an antiferromagnetic interaction can also be deduced from the $M(H)$ curves (Figure 2, b), in which the magnetization M versus the magnetic field H is only slightly S-shaped for magnetic fields above 20 kOe even at the lowest temperature of 1.8 K. This is not compatible with paramagnetic behavior and a Brillouin function for localized magnetic moment that corresponds to spin 3/2, as shown by a dashed curve in Figure 2 (b).

A detailed investigation of the susceptibility below 20 K (inset in Figure 2, a) shows a maximum of $\chi(T)$ at T_{max} = 2.6 K for **2**, whereas in **1** the maximum was not reached down to the lowest experimentally obtained temperature of 1.8 K. The maximum in susceptibility is a clear demonstration of the antiferromagnetic interaction between the magnetic moments of Co^{II} ions. However, a relatively round maximum of $\chi(T)$ without a sharp phase transition, no difference between zero-field and field-cooled susceptibilities (see inset in Figure 2, b), and the low temperature of T_{max} signify that the antiferromagnetic interaction must be weak and effective only between the four nearest Co^{II} ions in a molecular unit.

In addition to the antiferromagnetic interaction, the single-ion effects of the Co^{II} ions – mainly spin–orbit coupling[20] – should be taken into account when trying to describe the deviation of susceptibility from perfect paramagnetic behavior [i.e., a constant χT product and Brillouin-shaped $M(H)$]. Because both contributions are present simultaneously, modeling the measured susceptibility becomes very difficult. A similar temperature dependence of the χT product can be attributed either to the

antiferromagnetic interaction parameter J or to the spin–orbit coupling constant λ.

To further investigate the interactions in the Br sample, for which a maximum was observed in the susceptibility at low temperatures, simulations using PHI software[24] were performed. The Co ions in the double-cubane structure are coupled through superexchange interactions. To determine the distances between Co ions and Co–O–Co angles, a simplified spin-coupling diagram was constructed (Figure 3) on the basis of a simple interaction Hamiltonian:

$$H_{int} = -J_1 \cdot (S_1S_2 + S_1S_4 + S_2S_3 + S_2S_3) - J_2 \cdot S_3S_4$$

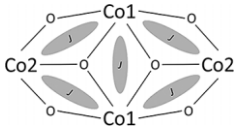

Figure 3. Simplified spin-coupling diagram for the Br sample showing the Co ions at two different sites and the double oxygen bridges.

The temperature dependence of the susceptibility data up to 20 K measured under 1000 Oe and the magnetization curve at 3 K were fitted simultaneously using four $S_i = 3/2$ spins coupled as shown in Figure 3. Although a simplified model was used, neglecting the spin–orbit coupling, the main feature of the susceptibility curve (namely, the maximum at 2.6 K), was reproduced (Figure 4). Furthermore, an excellent agreement of the simulated magnetization curve and experimental measurements was achieved. Coupling constants of $J_1 = -0.77$ cm^{-1} and $J_2 = -0.83$ cm^{-1} were obtained, which is in agreement with a weak antiferromagnetic interaction between Co^{II} ions. The discrepancy between the measured data and the fitted curve that increases at temperatures above 8 K might be attributed to the spin–orbit coupling we ignored in the fit.

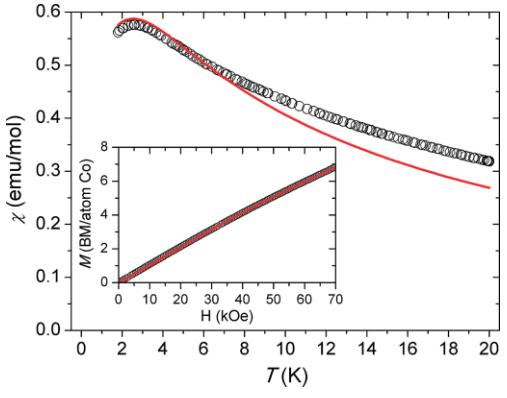

Figure 4. Temperature dependence of the susceptibility of **2** measured under 1000 Oe (circles) and the simulated curve (red line). The inset shows the magnetization curve of **2** (circles) and the curve obtained by simulation (red line) at 3 K.

Additionally, ac measurements were performed on **2**. Maximums in the in-phase ac susceptibility at temperatures independent (or very weakly dependent) of frequency and almost constant out-of-phase components of the ac susceptibility suggest that no single-molecule magnetism is present in this system (Figure 5).

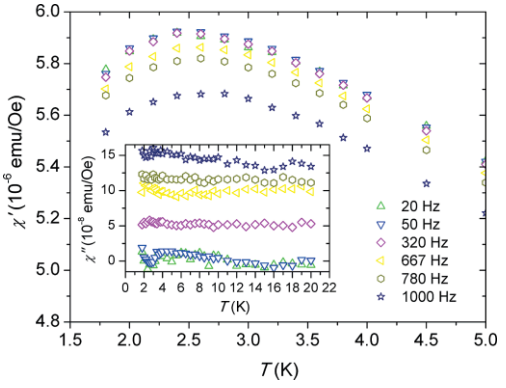

Figure 5. Temperature dependence of the in-phase component of the ac susceptibility χ' of **2** measured under 2 Oe at various frequencies. The inset shows the out-of-phase component of ac susceptibility χ''.

Preliminary Visible-Light-Driven Water Oxidation by 1 and 2

In typical photocatalytic water oxidation experiments for **1** and **2**, irradiation of **1** and **2** in aqueous borate buffer that contained 9 mM $K_2S_2O_8$ as sacrificial oxidant and 1 mM $[Ru(bpy)_3]Cl_2$ as photosensitizer were performed with an LED lamp at λ = 450 nm. In control experiments performed in the absence of one of the factors such as light, $K_2S_2O_8$, $[Ru(bpy)_3]Cl_2$, or Co clusters, we found that no O_2 production could be detected, which suggests that all components are prerequisites for light-driven O_2 production in our system (Figure S4 in the Supporting Information). Three different pH environments were evaluated for oxygen-evolution performance. Owing to the insolubility of **1** and **2** in such a reaction system, 2 mg of each solid sample was taken for tests every time. Photocatalytic oxygen generation was monitored through the detection of dissolved O_2 using a Clark-type electrode. As shown in Figure 6, the O_2 evolution with **1** and **2** increases steadily with irradiation time, then gradually reaches the maximum at around 1 min. The initial rate of O_2 evolution was obtained on the basis of the slope of the initial linear portion of the plots in Figure 6 (a and c). For **1**, the initial rates of O_2 evolution are 8.30, 11.36, and 9.30 mmol s^{-1} g^{-1} at pH = 7.4, 8.0, and 9.0, respectively (Figure 6, b), whereas these values under the same conditions are only 1.82, 2.18, and 0.91 mmol s^{-1} g^{-1} for **2** (Figure 6, d). Thus, the best oxygen-generation pH value of borate aqueous solution is 8 for both **1** and **2**. As the driving force for water oxidation increased at higher pH but was accompanied by the easy decomposition of the photosensitizer,[25] this might be why similar results can be seen in a 3d–4f $\{Co^{II}_3Ln(OR)_4\}$ cubane-catalyzed water oxidation system.[26] The overall photocatalytic efficiency of **1** is clearly superior to that of **2**, which is probably caused by manifold competing factors involved in oxygen evolution but is most likely related to the coordination differences between Cl and Br. The mechanism of water oxidation catalyzed by **1** and **2** is the focus of ongoing investigation but is difficult to determine on the basis of the data presented above. At any rate, a preliminary mechanistic framework could be proposed as shown in Scheme 2. In particular, the equilibria of halogen anion coordination and the nucleophilic attack by water could generate metal–water intermediates, which are then oxidized

to high-valent metal-oxo species by means of multielectron transfer. Hydrolysis of the high-valent intermediate species along with proton transfers would liberate O_2 and then close the catalytic cycle.[27] Thus, the free water molecule should be involved in the formation of the O–O bond, which suggests that the most likely mechanism should follow the water nucleophilic attack (WNA).[28] Such similar clusters with clearly different catalytic abilities provides evidence that water oxidation catalysis is mainly controlled by molecular species **1** and **2**. However, it is indeed difficult to completely exclude the free Co^{II} ions or CoO_x or $Co(OH)_x$ nanoparticles from the water oxidation catalysis activity.

To identify the mechanism behind the photocatalytic differences, spin-polarized DFT calculations were conducted using the DMol3 module.[29] The initial structures, which were derived from X-ray diffraction analysis, were first optimized without any constraints. Essentially, the Cl^- or Br^- ions were removed from the Co_4Cl_2 or Co_4Br_2 core to expose the catalytically active sites.

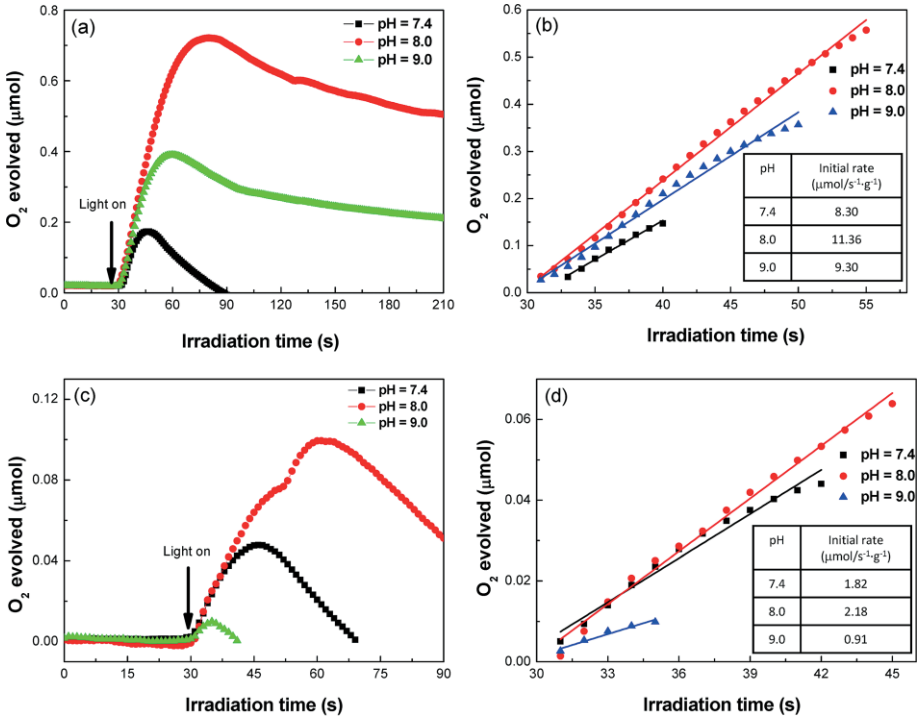

Figure 6. Photocatalytic oxygen evolution as a function of time from a 2 mL of solution containing 2 mg of (a) **1** and (c) **2** with $[Ru(bpy)_3]^{2+}$ (1 mM) and $K_2S_2O_8$ (9 mM) in borate buffer upon light irradiation (λ = 450 nm, 48 W). The kinetics of O_2 evolution rates of (b) **1** and (d) **2** based on linear fitting of the linear portion of the plots in (a) and (c), respectively.

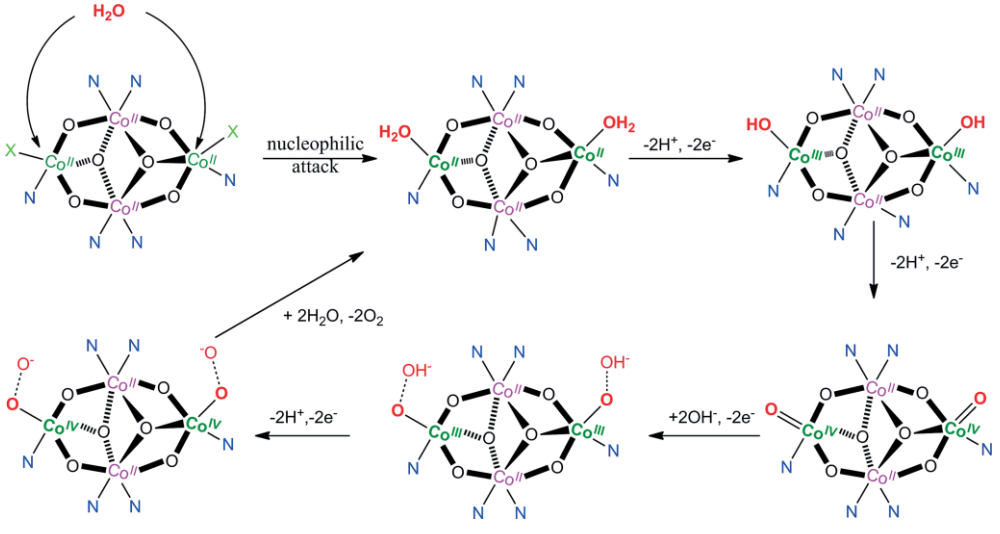

Scheme 2. Proposed catalytic cycle for water oxidation catalyzed by **1** or **2**.

In this way, the stable configurations of Co_4Cl^+ and Co_4Br^+ were identified. The gap between the highest occupied molecular orbital (HOMO) and the lowest unoccupied molecular orbital (LUMO) were 0.73 eV for Co_4Cl^+ and 0.62 eV for Co_4Br^+, which hints at the greater stability of Co_4Cl^+ over Co_4Br^+ ions. Inspection of the frontier molecular orbitals of Co_4Cl^+ and Co_4Br^+ ions reveals that both HOMOs consist of d_{z^2} orbitals of the middle two Co^{2+} ions, and $2p_z$ orbitals of O and N atoms of the ligands, whereas both of the LUMOs concentrate on d_{z^2} orbitals of one terminal pentacoordinate Co^{II} ion, a few $2p_z$ orbitals of O and N atoms, and π^* antibonding orbitals of one pyrazole group, as shown in Figure 7. Essentially, d_{z^2} orbitals in the LUMO act like Lewis acid active sites. Upon exposure to light, electrons can transfer from the pyrazole groups to the d_{z^2} orbitals and further donate to H_2O molecules. To examine the adsorption of H_2O, it is usually helpful to understand the difference in photocatalytic properties. Therefore we further identified the adsorption energy of H_2O on the catalysts. The E_{ad} value of 0.19 eV for Co_4Cl^+ is much larger than that of Co_4Br^+ (0.17 eV). It can be observed that H_2O molecules prefer to adsorb onto Co_4Cl^+ rather than Co_4Br^+ and thereby enhance the possibility of activating H_2O in Co_4Cl^+. By comparing the catalyst stability and the adsorption energy of H_2O of the two catalysts, we can satisfactorily posit that the photocatalytic properties of Co_4Cl^+ are better than that of Co_4Br^+.

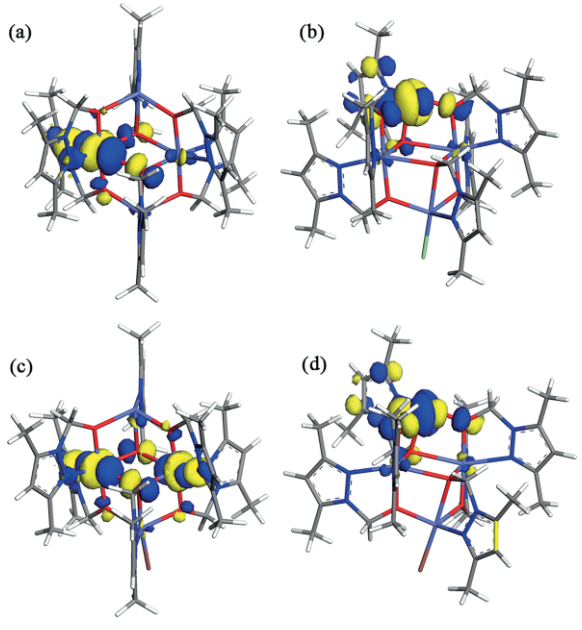

Figure 7. Frontier molecular orbitals: (a) HOMO and (b) LUMO of Co_4Cl^+. (c) HOMO and (d) LUMO of Co_4Br^+.

Electrical Conductivities of 1 and 2

In contrast to the widely studied properties of the coordination clusters, semiconductivity or conductivity is functionality that has long been sought after but is hard to access in cluster compounds owing to their intrinsic discrete characteristics, including dense packing in the solid state, and the lack of a continuous 1D, 2D, or 3D electron-transport pathway such as that found in some MOF materials.[30] However, the "through-space approach"[31] renews the possibility that the cluster compounds are semiconductive or even conductive. The electrical conductivity properties of **1** and **2** were assessed using a two-probe dc measurement on compressed pellets of polycrystalline samples. The *I*–*V* curves were plotted in the range of –20 to 20 V by using an Agilent B1500A semiconductor parameter analyzer at room temperature. As shown in Figure 8, the *I*–*V* curves follow Ohm's law as indicated by their good linearity; the currents were able to reach the nanoampere order in the measured voltage range, which suggests semiconductive behavior with a conductivity of 1.78×10^{-9} S cm^{-1} for **1** and 2.91×10^{-9} S cm^{-1} for **2**. These values are lower than that for many chalcogen-containing coordination compounds.[32] However, their intrinsic conductivities could be modulated and enhanced by guest molecule doping, which has been responsible for the huge success of conductive polymers.[33] The outstanding breakthrough in MOFs that was achieved by such a strategy is 7,7,8,8-tetracyanoquinodimethane (TCNQ)-doped HKUST-1, which displayed tunable conductivity from 10^{-8} to 0.07 S cm^{-1}.[34] In spite of such advances through this doping strategy in the field of coordination compounds, its application is not very extensive and the related mechanism is still unclear.[35] The conductivity performances of **1** and **2** can be further enhanced through a simple doping process in which the compounds and iodine are mechanically mixed by grinding in a mortar. For **1**, the conductivity values gradually increase from 5.8×10^{-7} to 4.7×10^{-4} and to a maximum of 5.4×10^{-4} S cm^{-1} as the I_2 mass fraction increases from 5 to 10 and to 15 %. A further increase in doped I_2 to 20 wt.-% conversely decreases the conductivity to 1.4×10^{-4} S cm^{-1} (inset plot in Figure 8, a). A similar conductiv-

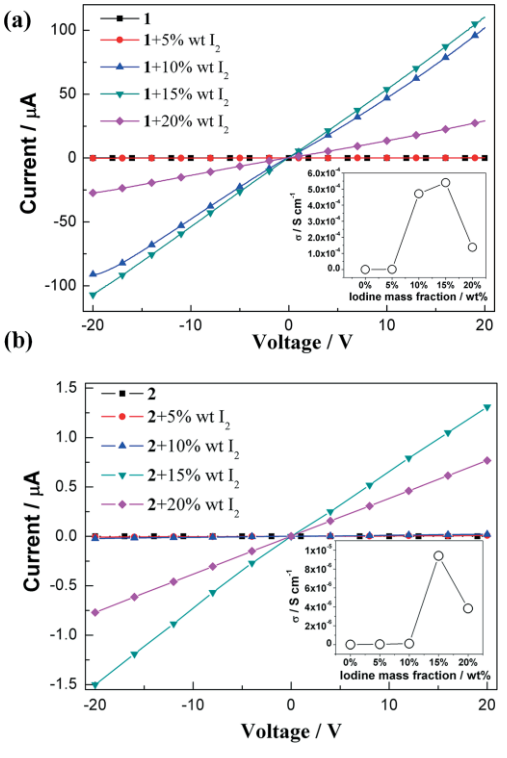

Figure 8. *I*–*V* curves of (a) **1** and (b) **2** with different amounts of I_2 doping.

ity evolution upon I_2 doping is also observed for **2**. The maximum conductivity increments between undoped and doped (15 %) **1** and **2** are 5 and 3 orders of magnitude, respectively. It is worth noting that conductivity boosts are an emergent functionality that are observed neither in tetranuclear Co clusters nor in the iodine molecules. The I_2 doping that induced better conductive performance should follow an oxidative doping mechanism that could produce a highly efficient n→σ* charge transfer,[36] as evidenced by the gradually enhanced absorption band above 700 nm relative to the undoped sample (Figure S6 in the Supporting Information).

Conclusion

We have isolated and structurally characterized two new tetranuclear cobalt(II) clusters with a face-shared open bicubane structural motif. An intramolecular antiferromagnetic interaction between four Co^{II} atoms is confirmed by magnetic susceptibility measurements. More interestingly, although the core motif of **1** and **2** is not classic Co_4O_4 monocubane, both of them are intrinsically active catalysts for water oxidation, and their relative O_2-evolution rates are dependent on the halogen terminal ligands. The electrical conductivity measurements gave the intrinsic σ value of approximately 10^{-9} S cm^{-1} at room temperature, thus indicating their semiconductive behavior. Interestingly, mechanical iodine doping was able to enhance the conductivity to approximately 10^{-4} S cm^{-1} relative to the undoped samples. The present work presents a new model of a molecular cobalt cluster-based photocatalytic water oxygen catalyst, provides new insight into the catalysis-related mechanism by comparing oxygen-evolution efficiency, and applies the iodine-doping strategy to boost the conductivity of cluster compounds.

Experimental Section

Materials and Methods: Commercially available solvents and metal salts were used without further purification. The ligand 1-(hydroxymethyl)-3,5-dimethylpyrazole was synthesized by the reaction of 3,5-dimethylpyrazole and paraformaldehyde as described by Driessen[37] and used after crystallization from CH_3CN. IR spectra were recorded using a PerkinElmer Spectrum Two in the frequency range of 4000–400 cm^{-1}. Elemental analyses for C, N, and H were performed using a PerkinElmer 2400 CHN elemental analyzer. Powder X-ray diffraction (PXRD) data were collected using a Philips X' Pert Pro MPD X-ray diffractometer with Mo-K_α radiation equipped with an X'Celerator detector. Thermogravimetric analyses (TGA) were performed using a SHIMADZU DTG-60A thermal analyzer from room temperature to 800 °C under a nitrogen atmosphere at a heating rate of 10 °C min^{-1}. The diffuse-reflectance spectrum was determined using a UV/Vis spectrophotometer (Evolution 220, ISA-220 accessory, Thermo Scientific) with a built-in 10 mm silicon photodiode with a 60 mm Spectralon sphere. Variable-temperature magnetic susceptibilities were collected using a magnetic property measurement system (MPMS), SQUID-VSM (superconducting quantum interference device-vibrating sample magnetometer) (Quantum Design, USA).

Photocatalytic Water Oxidation: The amount of evolved O_2 dissolved in solution was measured in situ by means of a standard Clark-type oxygen electrode (Hansatech Instruments). The electrode was calibrated following standard procedures before measurements. In a typical experiment, each component was mixed in buffer solution, then degassed with argon for 30 min. The degassed solution was then irradiated using a 450 nm LED lamp. The amount of O_2 evolved in solution was measured in situ.

Electrical Conductivity Measurement: The dc current–voltage (*I*–*V*) measurements were performed at room temperature using a two-probe method with an Agilent B1500A semiconductor parameter analyzer. Compressed circular pellet samples were made as follows: Single crystals of **1** and **2** were ground and pressed into pellets 0.4 cm in diameter and with thicknesses of 0.04–0.07 cm. The measurements were performed on these circular pellet samples with silver paint coated on both sides as electrodes. We repeated the experiments on samples with different thicknesses. The observed results are consistent within experimental errors.

Synthesis of Clusters 1 and 2: A mixture of $CoCl_2{\cdot}6H_2O$ (0.25 mmol, 72 mg) or $CoBr_2{\cdot}4H_2O$ (0.25 mmol, 83 mg) and HL (0.5 mmol, 61 mg) were dissolved in acetonitrile (5 mL), then triethylamine (60 μL) was added with a pipette. Afterwards, the resulting mixtures were sealed in a 25 mL Teflon-lined stainless steel autoclave and heated at 60 °C for 3500 min, after which the mixtures were cooled over 500 min to room temperature. The products were obtained as deep blue-purple rodlike crystals in yields of 70 and 85 % (based on cobalt) for **1** and **2**, respectively. For **1**: Selected IR peaks: $\tilde{\nu}$ = 3058 (w), 2936 (w), 2869 (w), 1672 (m), 1485 (m), 1435 (m), 1383 (m), 1366 (m), 1265 (m), 1150 (m), 1103 (m), 1020 (m), 1010 (m), 826 (m), 741 (s), 694 (s), 632 (s), 548 (m), 508 (s), 479 (m), 453 (m) cm^{-1}. Elemental analysis calcd. (%): C 40.89, H 5.15, N 15.89; found C 40.77, H 5.50, N 15.75. For **2**: Selected IR peaks: $\tilde{\nu}$ = 2988 (w), 2827 (w), 2741 (w), 1545 (m), 1490 (m), 1455 (m), 1406 (m), 1364 (m), 1239 (m), 1148 (m), 1119 (s), 1037 (m), 982 (m), 829 (m), 801 (m), 777 (m), 685 (s), 663 (m), 627 (m), 594 (m), 554 (m), 486 (m) cm^{-1}. Elemental analysis calcd. (%): C 37.72, H 4.75, N 14.66; found C 37.50, H 4.88, N 14.76. Crystal data for **1** and **2** are provided in Table 1. Selected bond lengths and angles are shown in Table S1 of the Supporting Information.

Table 1. Crystal data for **1** and **2**.

	1	**2**
Formula	$C_{36}H_{54}Cl_2Co_4N_{12}O_6$	$C_{36}H_{54}Br_2Co_4N_{12}O_6$
M_r	1057.55	1146.45
T [K]	298(2)	298(2)
Crystal system	monoclinic	monoclinic
Space group	$P2_1/n$	$P2_1/n$
a [Å]	10.4457(8)	10.565(3)
b [Å]	18.4395(15)	18.662(4)
c [Å]	11.6468(10)	11.445(3)
β [°]	96.384(6)	95.689(3)
V [Å^3]	2229.4(3)	2245.4(9)
Z	2	2
$\varrho_{calcd.}$ [g cm^{-3}]	1.5753	1.6955
μ [mm^{-1}]	1.635	3.278
F(000)	1091.7	1162.1
Reflections collected	23253	9347
Independent reflections	3925 [R_{int} = 0.0445]	4408 [R_{int} = 0.0533]
Data/parameters	3925/276	4408/275
GoF on F^2	1.049	1.002
Final R indexes [$I \geq 2\sigma(I)$]	R_1 = 0.0323, wR_2 = 0.0680	R_1 = 0.0470, wR_2 = 0.0821
Final R indexes [all data]	R_1 = 0.0530, wR_2 = 0.0763	R_1 = 0.1062, wR_2 = 0.1006
Largest diff. peak/hole [e Å^{-3}]	0.47/–0.41	1.07/–0.82

CCDC 1450527 (for **1**), and 1450528 (for **2**) contain the supplementary crystallographic data for this paper. These data can be obtained free of charge from The Cambridge Crystallographic Data Centre.

Supporting Information (see footnote on the first page of this article): Tables of crystal data in CIF files; details on IR, UV/Vis, TGA, and DFT calculations; powder X-ray diffractogram.

Acknowledgments

This work was supported by the National Natural Science Foundation of China (NSFC) (grant number 21571115), the Research Award Fund for Outstanding Middle-aged Young Scientist of Shandong Province (grant number BS2013CL010), the Young Scholars Program of Shandong University (grant number 2015WLJH24), The Fundamental Research Funds of Shandong University (grant numbers 104.205.2.5 and 2015JC045), and the Slovenian Research Agency (ARRS) (program number P2-0348).

Keywords: Cluster compounds · Cobalt · Water splitting · Magnetic properties · Semiconductivity · Doping

[1] G. A. Timco, S. Carretta, F. Troiani, F. Tuna, R. J. Pritchard, C. A. Muryn, E. J. L. McInnes, A. Ghirri, A. Candini, P. Santini, G. Amoretti, M. Affronte, R. E. P. Winpenny, *Nat. Nanotechnol.* **2009**, *4*, 173.

[2] L. Bogani, W. Wernsdorfer, *Nat. Mater.* **2008**, *7*, 179.

[3] a) Y. Z. Zheng, M. Evangelisti, F. Tuna, R. E. P. Winpenny, *J. Am. Chem. Soc.* **2012**, *134*, 1057; b) Y. Z. Zheng, M. Evangelisti, R. E. P. Winpenny, *Angew. Chem. Int. Ed.* **2011**, *50*, 3692; *Angew. Chem.* **2011**, *123*, 3776; c) Y. Z. Zheng, M. Evangelisti, R. E. P. Winpenny, *Chem. Sci.* **2011**, *2*, 99; d) Y. Z. Zheng, E. M. Pineda, M. Helliwell, R. E. P. Winpenny, *Chem. Eur. J.* **2012**, *18*, 4161; e) Y. Z. Zheng, G. J. Zhou, Z. P. Zheng, R. E. P. Winpenny, *Chem. Soc. Rev.* **2014**, *43*, 1462.

[4] R. Bagai, G. Christou, *Chem. Soc. Rev.* **2009**, *38*, 1011.

[5] a) A. Baniodeh, I. J. Hewitt, V. Mereacre, Y.-H. Lan, G. Novitchi, C. E. Anson, A. K. Powell, *Dalton Trans.* **2011**, *40*, 4080; b) W.-G. Wang, A.-J. Zhou, W.-X. Zhang, M.-L. Tong, X.-M. Chen, M. Nakano, C. C. Beedle, D. N. Hendrickson, *J. Am. Chem. Soc.* **2007**, *129*, 1014; c) A. J. Tasiopoulos, A. Vinslava, W. Wernsdorfer, K. A. Abboud, G. Christou, *Angew. Chem. Int. Ed.* **2004**, *43*, 2117; *Angew. Chem.* **2004**, *116*, 2169; d) Z.-M. Zhang, S. Yao, Y.-G. Li, R. Clérac, Y. Lu, Z.-M. Su, E.-B. Wang, *J. Am. Chem. Soc.* **2009**, *131*, 14600; e) P. Alborés, E. Rentschler, *Angew. Chem. Int. Ed.* **2009**, *48*, 9366; *Angew. Chem.* **2009**, *121*, 9530; f) D. Fenske, J. O. J. Hachgenei, *Angew. Chem. Int. Ed. Engl.* **1985**, *24*, 993; *Angew. Chem.* **1985**, *97*, 993; g) X.-J. Kong, Y.-L. Wu, L.-S. Long, L.-S. Zheng, Z.-P. Zheng, *J. Am. Chem. Soc.* **2009**, *131*, 6918; h) X.-J. Kong, L.-S. Long, R.-B. Huang, L.-S. Zheng, T. D. Harrisc, Z.-P. Zheng, *Chem. Commun.* **2009**, *29*, 4354.

[6] a) M. D. Kärkäs, O. Verho, E. V. Johnston, B. Åkermark, *Chem. Rev.* **2014**, *114*, 11863; b) S. Berardi, S. Drouet, L. Francas, C. Gimbert-Surinach, M. Guttentag, C. Richmond, T. Stoll, A. Llobet, *Chem. Soc. Rev.* **2014**, *43*, 7501; c) T. Zhang, W. Lin, *Chem. Soc. Rev.* **2014**, *43*, 5982; d) P. Du, R. Eisenberg, *Energy Environ. Sci.* **2012**, *5*, 6012; e) E. A. Karlsson, B.-L. Lee, T. Akermark, E. V. Johnston, M. D. Karkas, J. Sun, O. Hansson, J.-E. Backvall, B. Akermark, *Angew. Chem. Int. Ed.* **2011**, *50*, 11715; *Angew. Chem.* **2011**, *123*, 11919.

[7] a) A. Zouni, H. T. Witt, J. Kern, P. Fromme, N. Krauss, W. Saenger, P. Orth, *Nature* **2001**, *409*, 739; b) K. N. Ferreira, T. M. Iverson, K. Maghlaoui, J. Barber, S. Iwata, *Science* **2004**, *303*, 1831; c) Y. Umena, K. Kawakami, J.-R. Shen, N. Kamiya, *Nature* **2011**, *473*, 55.

[8] a) K. Jin, J. Park, J. Lee, K. D. Yang, G. K. Pradhan, U. Sim, D. Jeong, H. L. Jang, S. Park, D. Kim, N.-E. Sung, S. H. Kim, S. Han, K. T. Nam, *J. Am. Chem. Soc.* **2014**, *136*, 7435; b) X.-B. Han, Y.-G. Li, Z.-M. Zhang, H.-Q. Tan, Y. Lu, E.-B. Wang, *J. Am. Chem. Soc.* **2015**, *137*, 5486; c) A. K. Poulsen, A. Rompel, C. J. McKenzie, *Angew. Chem. Int. Ed.* **2005**, *44*, 6916; *Angew. Chem.* **2005**, *117*, 7076; d) S. Mukhopadhyay, S. K. Mandal, S. Bhaduri, W. H. Armstrong, *Chem. Rev.* **2004**, *104*, 3981.

[9] C. Zhang, C. Chen, H. Dong, J.-R. Shen, H. Dau, J. Zhao, *Science* **2015**, *348*, 690.

[10] a) R. Lalrempuia, N. D. McDaniel, H. Mueller-Bunz, S. Bernhard, M. Albrecht, *Angew. Chem. Int. Ed.* **2010**, *49*, 9765; *Angew. Chem.* **2010**, *122*, 9959; b) Y. Jiang, F. Li, B. Zhang, X. Li, X. Wang, F. Huang, L. Sun, *Angew. Chem. Int. Ed.* **2013**, *52*, 3398; *Angew. Chem.* **2013**, *125*, 3482; c) K. S. Joya, N. K. Subbaiyan, F. D'Souza, H. J. M. de Groot, *Angew. Chem. Int. Ed.* **2012**, *51*, 9601; *Angew. Chem.* **2012**, *124*, 9739; d) M. D. Karkas, T. Akermark, H. Chen, J. Sun, B. Akermark, *Angew. Chem. Int. Ed.* **2013**, *52*, 4189; *Angew. Chem.* **2013**, *125*, 4283; e) S. Maji, L. Vigara, F. Cottone, F. Bozoglian, J. Benet-Buchholz, A. Llobet, *Angew. Chem. Int. Ed.* **2012**, *51*, 5967; *Angew. Chem.* **2012**, *124*, 6069; f) Y. Xu, A. Fischer, L. Duan, L. Tong, E. Gabrielsson, B. Akermark, L. Sun, *Angew. Chem. Int. Ed.* **2010**, *49*, 8934; *Angew. Chem.* **2010**, *122*, 9118; g) J. D. Blakemore, N. D. Schley, D. Balcells, J. F. Hull, G. W. Olack, C. D. Incarvito, O. Eisenstein, G. W. Brudvig, R. H. Crabtree, *J. Am. Chem. Soc.* **2010**, *132*, 16017; h) F. Bozoglian, S. Romain, M. Z. Ertem, T. K. Todorova, C. Sens, J. Mola, M. Rodriguez, I. Romero, J. Benet-Buchholz, X. Fontrodona, C. J. Cramer, L. Gagliardi, A. Llobet, *J. Am. Chem. Soc.* **2009**, *131*, 15176; i) L. Duan, A. Fischer, Y. Xu, L. Sun, *J. Am. Chem. Soc.* **2009**, *131*, 10397; j) U. Hintermair, S. W. Sheehan, A. R. Parent, D. H. Ess, D. T. Richens, P. H. Vaccaro, G. W. Brudvig, R. H. Crabtree, *J. Am. Chem. Soc.* **2013**, *135*, 10837; k) A. R. Howells, A. Sankarraj, C. Shannon, *J. Am. Chem. Soc.* **2004**, *126*, 12258.

[11] a) X.-B. Han, Z.-M. Zhang, T. Zhang, Y.-G. Li, W. Lin, W. You, Z.-M. Su, E.-B. Wang, *J. Am. Chem. Soc.* **2014**, *136*, 5359; b) G. La Ganga, F. Puntoriero, S. Campagna, I. Bazzan, S. Berardi, M. Bonchio, A. Sartorel, M. Natali, F. Scandola, *Faraday Discuss.* **2012**, *155*, 177; c) F. Song, Y. Ding, B. Ma, C. Wang, Q. Wang, X. Du, S. Fua, J. Song, *Energy Environ. Sci.* **2013**, *6*, 1170; d) T. Nakazono, A. R. Parent, K. Sakai, *Chem. Commun.* **2013**, *49*, 6325; e) E. Pizzolato, M. Natali, B. Posocco, A. M. Lopez, I. Bazzan, M. Di Valentin, P. Galloni, V. Conte, M. Bonchio, F. Scandola, A. Sartorel, *Chem. Commun.* **2013**, *49*, 9941.

[12] a) V. Artero, M. Chavarot-Kerlidou, M. Fontecave, *Angew. Chem. Int. Ed.* **2011**, *50*, 7238; *Angew. Chem.* **2011**, *123*, 7376; b) N. S. McCool, D. M. Robinson, J. E. Sheats, G. C. Dismukes, *J. Am. Chem. Soc.* **2011**, *133*, 11446; c) S. Berardi, G. La Ganga, M. Natali, I. Bazzan, F. Puntoriero, A. Sartorel, F. Scandola, S. Campagna, M. Bonchio, *J. Am. Chem. Soc.* **2012**, *134*, 11104; d) M. D. Symes, D. A. Lutterman, T. S. Teets, B. L. Anderson, J. J. Breen, D. G. Nocera, *ChemSusChem* **2013**, *6*, 65; e) F. Evangelisti, R. Güttinger, R. Moré, S. Luber, G. R. Patzke, *J. Am. Chem. Soc.* **2013**, *135*, 18734; f) Z. Huang, Z. Luo, Y. V. Geletii, J. W. Vickers, Q. Yin, D. Wu, Y. Hou, Y. Ding, J. Song, D. G. Musaev, C. L. Hill, T. Lian, *J. Am. Chem. Soc.* **2011**, *133*, 2068; g) J. W. Vickers, H. Lv, J. M. Sumliner, G. Zhu, Z. Luo, D. G. Musaev, Y. V. Geletii, C. L. Hill, *J. Am. Chem. Soc.* **2013**, *135*, 14110.

[13] P. F. Smith, C. Kaplan, J. E. Sheats, D. M. Robinson, N. S. McCool, N. Mezle, G. C. Dismukes, *Inorg. Chem.* **2014**, *53*, 2113.

[14] a) B. Barszcz, T. Glowiak, J. Jezierska, A. Tomkiewicz, *Polyhedron* **2004**, *23*, 1309; b) F. Paap, E. Bouwman, W. L. Driessen, R. A. G. de Graaff, J. Reedijk, *J. Chem. Soc., Dalton Trans.* **1985**, *129*, 737.

[15] R. W. M. T. Hoedt, F. B. Hulsbergen, G. C. Verschoor, J. Reedijk, *Inorg. Chem.* **1982**, *21*, 2369.

[16] a) Z. E. Serna, M. K. Urtiaga, M. G. Barandika, R. Cortes, S. Martin, L. Lezama, M. I. Arriortua, T. Rojo, *Inorg. Chem.* **2001**, *40*, 4550; b) G. J. T. Cooper, G. N. Newton, P. Kogerler, D.-L. Long, L. Engelhardt, M. Luban, L. Cronin, *Angew. Chem. Int. Ed.* **2007**, *46*, 1340; *Angew. Chem.* **2007**, *119*, 1362; c) Y.-Z. Zhang, W. Wernsdorfer, F. Pan, Z.-M. Wang, S. Gao, *Chem. Commun.* **2006**, 3302; d) A. Ferguson, M. Schmidtmann, E. K. Brechin, M. Murrie, *Dalton Trans.* **2011**, *40*, 334; e) G. N. Newton, H. Sato, T. Shiga, H. Oshio, *Dalton Trans.* **2013**, *42*, 6701.

[17] a) J.-D. Leng, S.-K. Xing, R. Herchel, J.-L. Liu, M.-L. Tong, *Inorg. Chem.* **2014**, *53*, 5458; b) E. M. Pineda, F. Tuna, R. G. Pritchard, A. C. Regan, R. E. P. Winpenny, E. J. L. McInnes, *Chem. Commun.* **2013**, *49*, 3522; c) K. Su, F. Jiang, J. Qian, J. Pang, S. A. Al-Thabaiti, S. M. Bawaked, M. Mokhtar, Q. Chen, M. Hong, *Cryst. Growth Des.* **2014**, *14*, 5865; d) H. Xu, Q. Wang, J.-H. Qin, S.-Q. Zang, S. K. Langley, K. S. Murray, B. Moubaraki, S. R. Batten, T. C. W. Mak, *Chem. Commun.* **2015**. DOI: 10.1039/c5cc04401d; e) Q. Chen, M.-H. Zeng, Y.-L. Zhou, H.-H. Zou, M. Kurmoo, *Chem. Mater.* **2010**, *22*, 2114; f) Q. Chen, M.-H. Zeng, L.-Q. Wei, M. Kurmoo, *Chem. Mater.* **2010**, *22*, 4328; g) Y.-Q. Hu, M.-H. Zeng, K. Zhang, S. Hu, F.-F. Zhou, M. Kurmoo, *J. Am. Chem. Soc.* **2013**, *135*, 7901.

[18] A. W. Addison, T. N. Rao, J. Reedijk, J. Van Rijn, G. C. Verschoor, *J. Chem. Soc., Dalton Trans.* **1984**, 1349.
[19] G. A. Seisenbaeva, M. Kritikos, V. G. Kessler, *Polyhedron* **2003**, *22*, 2581.
[20] S. G. Telfer, R. Kuroda, J. Lefebvre, D. B. Leznoff, *Inorg. Chem.* **2006**, *45*, 4592.
[21] R. Pattacini, P. Teo, J. Zhang, Y. Lan, A. K. Powell, J. Nehrkorn, O. Waldmann, T. S. A. Hor, P. Braunstein, *Dalton Trans.* **2011**, *40*, 10526.
[22] O. Kahn, *Molecular Magnetism*, VCH Publishers, NewYork, **1993**.
[23] N. W.Ashcroft, N. D.Mermin, *Solid State Physics*, Saunders College Publishing, USA, **1976**.
[24] N. F. Chilton, R. P. Anderson, L. D. Turner, A. Soncini, K. S. Murray, *J. Comput. Chem.* **2013**, *34*, 1164.
[25] a) D. Hong, J. Jung, J. Park, Y. Yamada, T. Suenobu, Y.-M. Lee, W. Nam, S. Fukuzum, *Energy Environ. Sci.* **2012**, *5*, 7606; b) C. Creutz, N. Sutin, *Proc. Natl. Acad. Sci. USA* **1975**, *72*, 2858.
[26] F. Evangelisti, R. More, F. Hodel, S. Luber, G. R. Patzke, *J. Am. Chem. Soc.* **2015**, *137*, 11076.
[27] M. L. Rigsby, S. Mandal, W. Nam, L. C. Spencer, A. Llobet, S. S. Stahl, *Chem. Sci.* **2012**, *3*, 3058.
[28] X. Sala, S. Maji, R. Bofill, J. Garcia-Anton, L. Escriche, A. Llobet, *Acc. Chem. Res.* **2014**, *47*, 504.
[29] a) B. Delley, *J. Chem. Phys.* **1990**, *92*, 508; b) B. Delley, *J. Chem. Phys.* **2000**, *113*, 7756.
[30] a) L. Sun, M. G. Campbell, M. Dincá, *Angew. Chem. Int. Ed.* 10.1002/anie.201506219; b) T. Kambe, R. Sakamoto, K. Hoshiko, K. Takada, M. Miyachi, J. Ryu, S. Sasaki, J. Kim, K. Nakazato, M. Takata, H. Nishihara, *J. Am. Chem. Soc.* **2013**, *135*, 2462; c) Z. Zhang, H. Zhao, H. Kojima, T. Mori, K. R. Dunbar, *Chem. Eur. J.* **2013**, *19*, 3348.
[31] R. Hoffmann, *Acc. Chem. Res.* **1971**, *4*, 1.
[32] a) S. Takaishi, M. Hosoda, T. Kajiwara, H. Miyasaka, M. Yamashita, Y. Nakanishi, Y. Kitagawa, K. Yamaguchi, A. Kobayashi, H. Kitagawa, *Inorg. Chem.* **2009**, *48*, 9048; b) L. Sun, C. H. Hendon, M. A. Minier, A. Walsh, M. Dinca, *J. Am. Chem. Soc.* **2015**, *137*, 6164.
[33] C. K. Chiang, C. R. Fincher, Y. W. Park, A. J. Heeger, H. Shirakawa, E. J. Louis, S. C. Gau, A. G. MacDiarmid, *Phys. Rev. Lett.* **1977**, *39*, 1098.
[34] A. A. Talin, A. Centrone, A. C. Ford, M. E. Foster, V. Stavila, P. Haney, R. A. Kinney, V. Szalai, F. E. Gabaly, H. P. Yoon, F. Léonard, M. D. Allendorf, *Science* **2014**, *343*, 66.
[35] a) Y. Kobayashi, B. Jacobs, M. D. Allendorf, J. R. Long, *Chem. Mater.* **2010**, *22*, 4120; b) M. Zeng, Q. Wang, Y. Tan, S. Hu, H. Zhao, L. Long, M. Kurmoo, *J. Am. Chem. Soc.* **2010**, *132*, 2561; c) F. Gándara, F. J. Uribe-Romo, D. K. Britt, H. Furukawa, L. Lei, R. Cheng, X. Duan, M. O'Keeffe, O. M. Yaghi, *Chem. Eur. J.* **2012**, *18*, 10595.
[36] a) Z. Hao, G. Yang, X. Song, M. Zhu, X. Meng, S. Zhao, S. Song, H. Zhang, *J. Mater. Chem. A* **2014**, *2*, 237; b) S. T. Meek, J. A. Greathouse, M. D. Allendorf, *Adv. Mater.* **2011**, *23*, 249.
[37] W. L. Driessen, *Recl. Trav. Chim. Pays-Bas* **1982**, *101*, 441.

Received: May 2, 2016
Published Online: ■

Water Oxidation Catalysts

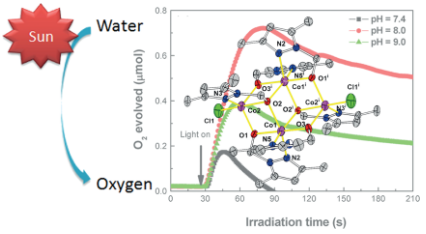

This work presents a new core type of cobalt cluster that possesses photocatalytic oxygen-evolution capabilities, provides new insight into the catalysis-related mechanism based on the relative oxygen evolution efficiency, and applies the iodine-doping strategy to boost the conductivity of cluster compounds.

DOI: 10.1002/ejic.201600510

